ELSEVIER

Journal of Organometallic Chemistry 632 (2001) 175–187

Journal of Organometallic Chemistry

www.elsevier.com/locate/jorganchem

Heptacoordinate dithiophosphate Mo(II) and W(II) complexes: molecular structures of mono and binuclear phosphine complexes

Huizhang Liu [a], Maria José Calhorda [a,b,*], Vitor Félix [c], Michael G.B. Drew [d]

[a] *Instituto de Tecnologia Química e Biológica (ITQB), Av. da República, EAN, Apt 127, 2781-901 Oeiras, Portugal*
[b] *Departamento de Química e Bioquímica, Faculdade de Ciências da Universidade de Lisboa, 1749-016 Lisbon, Portugal*
[c] *Departamento de Química, Universidade de Aveiro, 3810-193 Aveiro, Portugal*
[d] *Department of Chemistry, University of Reading, Whiteknights, Reading RG6 6AD, UK*

Received 15 March 2001; accepted 1 May 2001

Dedicated to Professor A. Romão Dias on the occasion of his 60th birthday

Abstract

The complex $[M(CO)_3\{S_2P(OEt)_2\}_2]$ (M = Mo, W) can be obtained in situ from the reaction of $[MI_2(CO)_3(NCMe)_2]$ with ammoniumdiethyldithiophosphate, in dichloromethane. One or two carbonyl groups can be replaced by mono and bidentate phosphines, such as $Ph_2PCH_2PPh_2$ (dppm), $Ph_2P(CH_2)_2PPh_2$ (dppe), or PPh_3, to afford heptacoordinate complexes $[M(CO)_2(PPh_3)\{S_2P(OEt)_2\}_2]$ (M = Mo, **2a**; W, **2b**), $[M(CO)_2\{S_2P(OEt)_2\}_2]_2(\mu$-dppe) (M = Mo, **3a**; W, **3b**), $[M(CO)(dppm)\{S_2P(OEt)_2\}_2]$ (M = Mo, **4a**; W, **4b**), $[Mo(CO)(dppe)\{S_2P(OEt)_2\}_2]$ (**5a**), $[W(CO)_2(dppe)\{S_2P(OEt)_2\}_2]$ (**6b**), and $[Mo(O)(I)(dppe)\{S_2P(OEt)_2\}]$ (**7a**). All these complexes, with the exception of **4b**, were structurally characterized by single crystal X-ray diffraction. The capped octahedral geometry was observed in all biscarbonyl species, the CO being the capping ligand. Complex **4a** exhibits a pentagonal bipyramidal arrangement, with the carbonyl occupying one axial position, while **7a** is an octahedral complex. These complexes were studied by cyclic voltammetry, showing essentially irreversible processes, involving orbitals with a strong d character.

Keywords: Molybdenum; DFT calculations; Allyl complexes; Crystal structures; Binuclear complexes

1. Introduction

Molybdenum plays an important role in metalloenzymes. In particular, it has been known for some time that nitrogenases contain a molybdenum center [1], but only recently, with the crystal structure determination of the active center of nitrogenase has its coordination environment been established [2]. Much uncertainty still remains about its precise function, though, and it is therefore important to acquire more knowledge on related molybdenum complexes where the metal is bound to sulfur ligands. Besides its role in nitrogen fixation, molybdenum associated with sulfur also plays an important role on hydrodesulfurization reactions [3]. The search for new molybdenum chemistry has led to the synthesis and study of a large variety of Mo(II) derivatives [4–6]. Heptacoordination of the metal is observed if the 18 electron count is achieved, as happens with most of the characterized compounds, although examples of unusual unsaturated 16 electron carbonyl derivatives are also known [4h]. The seven-coordinate complexes exhibit geometries ranging from the capped octahedron, capped trigonal prism, and pentagonal bipyramid, to the 4:3 geometry [4c]. These structures and their interconversions pathways have been examined in detail [7]. We describe the synthesis and properties of a family of new mixed carbonyl, phosphine and dithiophosphate Mo(II) and W(II) complexes, mono- and binuclear. Most of the compounds have been structurally characterized by single crystal X-ray diffraction.

* Corresponding author. Tel.: +351-21-446-9754; fax: +351-21-441-3969.
E-mail address: mjc@itqb.unl.pt (M.J. Calhorda).

0022-328X/01/$ - see front matter
PII: S0022-328X(01)00989-5

2. Results and discussion

2.1. Chemical results

The reaction of the well known complexes $[MI_2(CO)_3(NCMe)_2]$ (M = Mo, W) [4] with ammonium diethyldithiophosphate, in dichloromethane, led to the new species $[M(CO)_3\{S_2P(OEt)_2\}_2]$ (M = Mo (**1a**), W (**1b**)), a procedure related to that described by other authors [4h].

These materials were used as precursors in situ for all the other complexes, as shown in Scheme 1, which were prepared in reactions involving substitution of carbonyls by several different phosphines ($Ph_2PCH_2PPh_2$ = dppm; $Ph_2P(CH_2)_2PPh_2$ = dppe; PPh_3) in different proportions.

The reaction of **1a** with PPh_3 led to the substitution of one carbonyl, as suggested by the presence of two $\nu_{C\equiv O}$ stretching modes in **2a**, at 1939 and 1860 cm^{-1}, assigned to the symmetric and antisymmetric modes of two coordinated carbonyl groups. The ^{1}H-NMR spectrum in CD_3CN shows three broad peaks for the phenyl protons ($\delta = 7.41$ ppm), the methylenic protons of the ethyl group ($\delta = 1.28$ ppm), and the methylic protons of the ethyl group ($\delta = 4.11$ ppm), respectively, integrating approximately as 15:12:8, respectively. The peaks are too broad to allow for an accurate integration. The complex **2a** was confirmed by a single crystal X-ray study (see Section 2.2) as the heptacoordinate Mo(II) complex $[Mo(CO)_2(PPh_3)\{S_2P(OEt)_2\}_2]$. The same reaction was carried out, using the W analog as starting reagent. A similar product, **2b**, was obtained, which exhibited two $\nu_{C\equiv O}$ stretching modes at 1927 and 1840 cm^{-1}, and three ^{1}H-NMR peaks (multiplets) at δ 7.32–7.51 ppm, 1.26–1.31 ppm, and 4.14 ppm, for the phenyl, methylene, and methyl protons, respectively. This spectroscopic evidence and a single crystal X-ray study led to the assignment of this complex as $[W(CO)_2(PPh_3)\{S_2P(OEt)_2\}_2]$.

In the analogous reaction with dppe, a 2:1 ratio of **1a** (**1b**) to dppe was used, with the aim of obtaining binuclear complexes of Mo or W with bridging dppe. The products obtained (**3a**, **3b**) still exhibited two $\nu_{C\equiv O}$ stretching modes (1937, 1850 cm^{-1}, for Mo, and 1925, 1831 cm^{-1}, for W), suggesting that two carbonyl groups remained coordinated to the metal center. The ^{1}H-NMR spectra in CD_3CN show peaks assigned to phenyl protons ($\delta = 7.55$–7.62 for Mo, 7.59 for W), CH_2 from dppe ($\delta = 2.66$–2.73 for Mo, 2.66–2.72 for W), CH_2 from OEt ($\delta = 3.87$–4.28 for Mo, 3.96–4.24 for W), and CH_3 from OEt ($\delta = 1.12$–1.39 for Mo, 1.22–1.37 for W). These peaks are all broad multiplets making an integration extremely difficult. The structure of each compound was confirmed by single crystal X-ray diffraction studies to be a binuclear complex with the two metals bridged by a dppe ligand, $[M(CO)_2\{S_2P(OEt)_2\}_2]_2(\mu\text{-dppe})$.

The reaction of **1a** (**1b**) with dppm in a 1:1 ratio, should in principle lead to substitution of two carbonyls by the bidentate ligand. For Mo, one broad band at 1806 cm^{-1} with a shoulder is assigned to the $\nu_{C\equiv O}$ stretching mode. The ^{1}H-NMR spectrum in CD_3CN is compatible with the composition $[Mo(CO)(dppm)\{S_2P(OEt)_2\}_2]$ (**4a**), which was confirmed by X-ray diffraction studies. For the W complex, the band corresponding to the $\nu_{C\equiv O}$ stretching mode is partially split in two, at 1809 and 1790 cm^{-1}, but the IR spectrum is almost superimposable with that of **4a**. This split band is, however, quite distinct from the two well-defined bands observed for complexes **2a**, **2b**, **3a**, and **3b.** The IR spectrum of an acetonitrile solution of the complex was also recorded and showed only one band, indicating the coordination of only one carbonyl. Therefore, the complex can be formulated as $[W(CO)(dppm)\{S_2P(OEt)_2\}_2]$ (**4b**).

The reactions of **1a** (**1b**) with dppe in a 1:1 ratio were expected to follow similar trends. Indeed, for Mo, a sharp band at 1811 cm^{-1} indicated unequivocally the

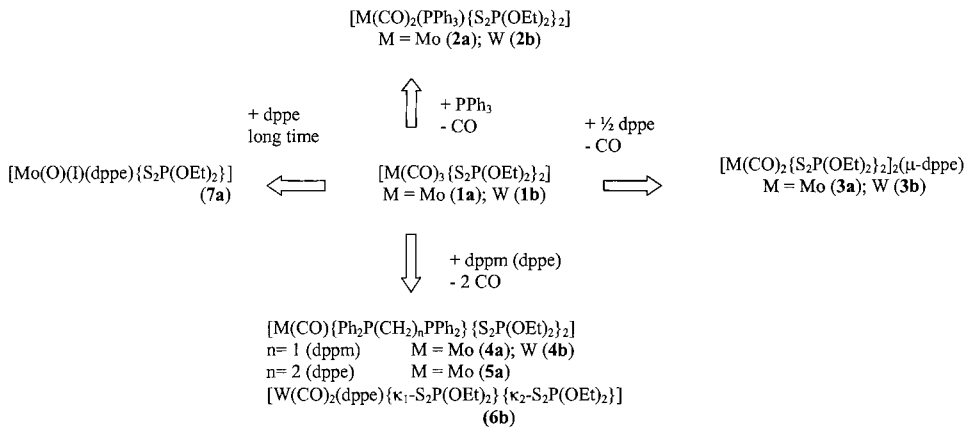

Scheme 1.

presence of only one coordinated carbonyl, the ^{1}H-NMR spectrum in CD_3CN being compatible with the formulation $[Mo(CO)(dppe)\{S_2P(OEt)_2\}_2]$ (**5a**). This structure was confirmed by single crystal X-ray diffraction. The IR spectrum of the complex, obtained when the same reaction was repeated with the W precursor, showed two well defined bands in the region of $\nu_{C\equiv O}$ stretching vibrations, at 1943 and 1862 cm^{-1}, suggesting that a different product might have been formed. The ^{1}H-NMR spectrum in CD_3CN is not of sufficient quality to assign another structure, since multiplets assignable to phenyl groups, methylene protons from dppe and OEt, and methyl protons are observed with chemical shifts comparable to those of the Mo complex **5a**. The single crystal X-ray study showed this new tungsten complex to be $[W(CO)_2(dppe)\{\kappa_1\text{-}S_2P(OEt)_2\}\text{-}\{\kappa_2\text{-}S_2P(OEt)_2\}]$ (**6b**), where one $S_2P(OEt)_2$ coordinates in the usual bidentate mode but the other is monodentate, so that the heptacoordination of the metal is maintained. In an attempt to prepare a second batch of **5a**, the reaction was repeated but accidentally the work up period was longer. In particular, the recrystallization period took place over a period of several days rather than overnight. Although the IR spectrum was surprisingly similar to that of **6b**, with two peaks at 1944 and 1879 cm^{-1}, the single crystal X-ray diffraction revealed a completely different compound, $[Mo(O)(I)(dppe)\text{-}\{S_2P(OEt)_2\}]$ (**7a**), without any coordinated carbonyl. From the reasons given above, namely badly defined multiplets, ^{1}H-NMR does not give much structural information. The most likely explanation is that a Mo analog of **6b** may form **6a** and under exposure to some air and water during the long crystallization process, oxidation to **7a** takes place. Indeed, compounds such as $[MI(CO)_2(dppe)\{S_2P(OEt)_2\}]$ [8], may be the intermediates in the oxidation to **7a**. Their presence may be assigned to incomplete removal of iodide in the parent precursor $[MI_2(CO)_3(NCMe)_2]$. There are possible equilibria between different species where bidentate ligands dppe and $S_2P(OEt)_2$ change their bonding mode, leading to expulsion of the second carbonyl. The final product is probably a mixture of **6a** and **7a**, as suggested by the IR spectrum, the crystal of **7a** having been selected. The intensity of the carbonyl stretching bands is much smaller than in all the other compounds.

2.2. Crystal structures

The structures of complexes $[Mo(CO)_2(PPh_3)\text{-}\{S_2P(OEt)_2\}_2]$ (**2a**), $[W(CO)_2(PPh_3)\{S_2P(OEt)_2\}_2]$ (**2b**), $[Mo(CO)_2\{S_2P(OEt)_2\}_2]_2(\mu\text{-dppe})$ (**3a**), $[W(CO)_2\text{-}\{S_2P(OEt)_2\}_2]_2(\mu\text{-dppe})$ (**3b**), $[Mo(CO)(dppm)\{S_2P\text{-}(OEt)_2\}_2]$ (**4a**), $[Mo(CO)(dppe)\{S_2P(OEt)_2\}_2]$ (**5a**), $[W(CO)_2(dppe)\{S_2P(OEt)_2\}_2]$ (**6b**), and $[Mo(O)(I)\text{-}(dppe)\{S_2P(OEt)_2\}]$ (**7a**), were determined by single crystal X-ray diffraction. The first six complexes all have seven-coordinate environments, while complex **7a**, obtained from an alternative process, is six-coordinate.

The crystal structures of **2a** and **2b** consist of discrete monomers molecules of $[Mo(CO)_2(PPh_3)\{S_2P(OEt)_2\}_2]$ (**2a**), and $[W(CO)_2(PPh_3)\{S_2P(OEt)_2\}_2]$ (**2b**), respectively. The bond lengths and angles in the metal coordination spheres are given in Table 1 for both complexes.

From a comparison of the unit-cell dimensions (see Table 6) and molecular geometry parameters, it is clear that these two complexes are isomorphous. The molecular structure of **2a** together with the atomic notation scheme used is shown in Fig. 1. **2b**, not shown, is equivalent. In each structure the metal center is coordinated to two carbonyls, four sulfur donor atoms from two dithiolate bidentate ligands, and one phosphorus atom of the triphenylphosphine ligand. The coordination polyhedra can be described as distorted capped octahedra. The carbonyl group comprising the atoms C(200) and O(200) occupies the capping position on the triangular face defined by the atoms S(4), P(7), and C(100), intersecting this face nearly on the perpendicular, at an angle of 88.6° for **2a** and **2b**. Atoms S(1), S(3), and S(6) occupy the uncapped face. The M–S(4) bond

Table 1
Bond lengths (Å) and angles (°) in the metal coordination spheres of **2a**, **2b**, **3a** and **3b**

	2a	**2b**	**3a**	**3b**
Bond lengths				
M–C(100)	1.937(10)	1.955(4)	1.934(16)	1.898(12)
M–C(200)	1.960(9)	1.935(4)	1.960(14)	1.947(13)
M–S(1)	2.599(3)	2.585(3)	2.595(5)	2.594(4)
M–S(4)	2.553(3)	2.551(3)	2.551(5)	2.535(4)
M–S(3)	2.651(3)	2.653(3)	2.659(4)	2.655(4)
M–S(6)	2.643(4)	2.620(4)	2.655(5)	2.637(4)
M–P(7)	2.520(3)	2.514(3)	2.513(4)	2.500(2)
Bond angles				
S(1)–M–S(3)	75.7(1)	76.4(1)	74.6(1)	74.4(1)
S(4)–M–S(3)	78.0(1)	76.7(1)	77.5(2)	76.8(1)
P(7)–M–S(4)	122.5(1)	123.5(1)	129.4(1)	129.6(1)
P(7)–M–S(1)	79.9(1)	79.3(1)	74.9(1)	75.2(1)
S(1)–M–S(4)	150.4(1)	149.6(1)	149.2(1)	148.0(1)
P(7)–M–S(3)	153.8(1)	153.7(18)	153.78(7)	148.6(1)
C(100)–M–S(6)	168.0(2)	167.6(1)	170.3(4)	170.0(3)
C(100)–M–C(200)	71.0(3)	70.9(2)	74.0(6)	72.8(5)
C(200)–M–S(6)	120.4(2)	121.3(1)	115.4(4)	116.9(3)
S(6)–M–S(4)	75.9(1)	76.3(1)	76.2(1)	76.1(1)
S(6)–M–S(1)	89.0(1)	87.9(1)	89.9(1)	88.8(1)
C(100)–M–P(7)	104.2(2)	103.8(1)	101.0(4)	101.5(3)
C(200)–M–P(7)	71.3(2)	72.1(1)	74.0(4)	74.4(3)
P(7)–M–S(6)	84.0(1)	83.8(1)	84.5(1)	84.2(1)
C(100)–M–S(1)	83.9(2)	84.0(1)	84.0(4)	84.8(3)
C(200)–M–S(1)	135.1(2)	135.3(1)	137.3(4)	137.3(3)
C(100)–M–S(4)	106.0(2)	106.6(1)	105.5(4)	105.6(3)
C(200)–M–S(4)	74.0(2)	74.6(1)	73.1(4)	74.4(3)
C(100)–M–S(3)	82.8(2)	83.4(1)	83.0(4)	83.4(3)
C(200)–M–S(3)	134.0(2)	133.4(1)	135.7(4)	135.6(3)
S(6)–M–S(3)	86.1(1)	85.6(1)	88.2(2)	87.4(1)

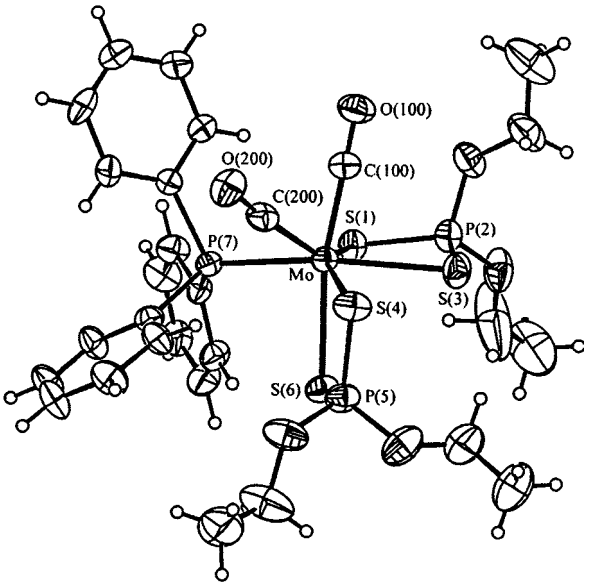

Fig. 1. An ORTEP view of $[Mo(CO)_2(PPh_3)\{S_2P(OEt)_2\}_2]$ (**2a**), with thermal ellipsoids drawn at 30% probability. The atom numbering scheme of the phenyl and ethoxy groups is omitted for clarity. The analogous tungsten complex **2b** is isomorphous.

to the sulfur atom in the capped face is the shortest bond. The next shortest bond is M–S(1), where S(1) is trans to S(4), rather than S trans to P(7) and C(100), as are S(3) and S(2), respectively.

The crystal structures of **3a** and **3b** consist of dimeric discrete molecules of $[Mo(CO)_2\{S_2P(OEt)_2\}_2]_2$(μ-dppe) (**3a**), and $[W(CO)_2\{S_2P(OEt)_2\}_2]_2$(μ-dppe) (**3b**), respectively. As for **2a** and **2b**, these two complexes are also isomorphous. The structures contain a crystallographic center of symmetry. A complete picture of the molecular structure of **3a** (**3b** is equivalent) is shown in Fig. 2a. The first molecular diagram is a general view of the overall structure of the molybdenum binuclear complex and Fig. 2b is a side view of the crystallographic asymmetric unit, emphasizing the geometry of the metal coordination polyhedron.

Two $M(CO)_2\{S_2P(OEt)_2\}_2$ structural units (M = Mo(II) or W(II)) are linked by a dppe bridge, which holds the two metal centers at 8.789(2) Å in **3a** and 8.783(1) Å in **3b**. The bridge adopts an *anti* conformation with a P–C–C–P torsion angle of 180° due to the presence of a crystallographic inversion center. The molecular dimensions of the two structural $M(CO)_2\{S_2P(OEt)_2\}_2$ fragments in these two complexes, also listed in Table 1, compare quite well with those found for the analogues **2a** and **2b**. In fact, the differences between the four X-ray determinations are less than 0.04 Å in bond lengths and 3° in the angles. Therefore, the complexes **3a** and **3b** also exhibit a capped octahedral geometry with identical disposition of the ligands. Furthermore, the capping carbonyl ligand is again almost perpendicular to the S(4), P(7), C(100) triangular face, making with it angles of 89.7° in **3a** and 89.6° in **3b**.

The crystal structure of **6b** consists of $[W(CO)_2(dppe)\{S_2P(OEt)_2\}_2]$ and CH_2Cl_2 crystallisation solvent molecules. Table 2 lists the selected bond lengths and angles for **6b** while Fig. 3 shows the molecular structure with the atomic numbering scheme adopted.

The tungsten center is bonded to two carbonyl groups, two phosphorus atoms from dppe, and three sulfur atoms of two thiolate ligands. The chelation of tungsten atom by two phosphorus donors of the dppe ligand prevents the coordination of a sulfur atom of the second $S_2P(OEt)_2$ bidentate ligand. The sulfur atom S(3) is clearly displaced from the tungsten coordination sphere, giving rise to a W–S(1)–P(2)–S(3) torsion angle of 137.6(3)° and an intermolecular distance S(3)···W of 5.478(6) Å. In addition, the P(2)–S(3) bond length of 1.938(6) Å is shorter than the remaining three P–S bond lengths of 2.014(6), 1.985(6) and 1.991(6) Å between phosphorus and coordinated sulfur atoms. Thus, the bond P(2)–S(3) retains some double bond character, while in the other three it is reduced by the coordination of their sulfur atoms to the metal center. Complex **6b** also exhibits a distorted capped octahedral geometry, with the carbonyl capping the triangular face defined by the atoms C(100), S(4) and P(7). The angle between the carbonyl group and the C(100), S(4), P(7) triangular face is 89.9°. The W–S, W–P and W–C distances are comparable to those for **2b** and **3b** and in addition it is apparent that W–P(7) in the capped face is much shorter at 2.480(4) Å than W–P(10) in the uncapped face at 2.568(4) Å.

The crystal structure of **4a** consists of discrete molecules of $[Mo(CO)(dppm)\{S_2P(OEt)_2\}_2]$ and CH_2Cl_2 solvent crystallization molecules, while that of **5a** only contains discrete molecules of $[Mo(CO)(dppe)\{S_2P(OEt)_2\}_2]$. Selected bond lengths and angles in the molybdenum coordination sphere are compared in Table 3. The molecular structures of **4a** and **5a**, together with atomic numbering scheme used are shown in Figs. 4 and 5, respectively.

In contrast with the five structures described above, the complexes **4a** and **5a** display a distorted pentagonal bipyramidal coordination environment around the molybdenum, with the equatorial coordination defined by three sulfur atoms of two $S_2P(OEt)_2$ bidentate ligands and two phosphorus atoms from dppm in **4a** or from dppe in **5a**. Seven coordination is completed with two axial atoms, the remaining sulfur of a $S_2P(OEt)_2$ ligand and the carbon atom of the carbonyl group, with a C(100)–Mo–S(6) angle of 172.30(20) and 169.90(30)°, respectively, in **4a** and **5a**. In both complexes, the atoms that define the equatorial plane show significant deviations from the least-squares plane calculated with their atomic positions. These deviations are in Å: −0.181(1)

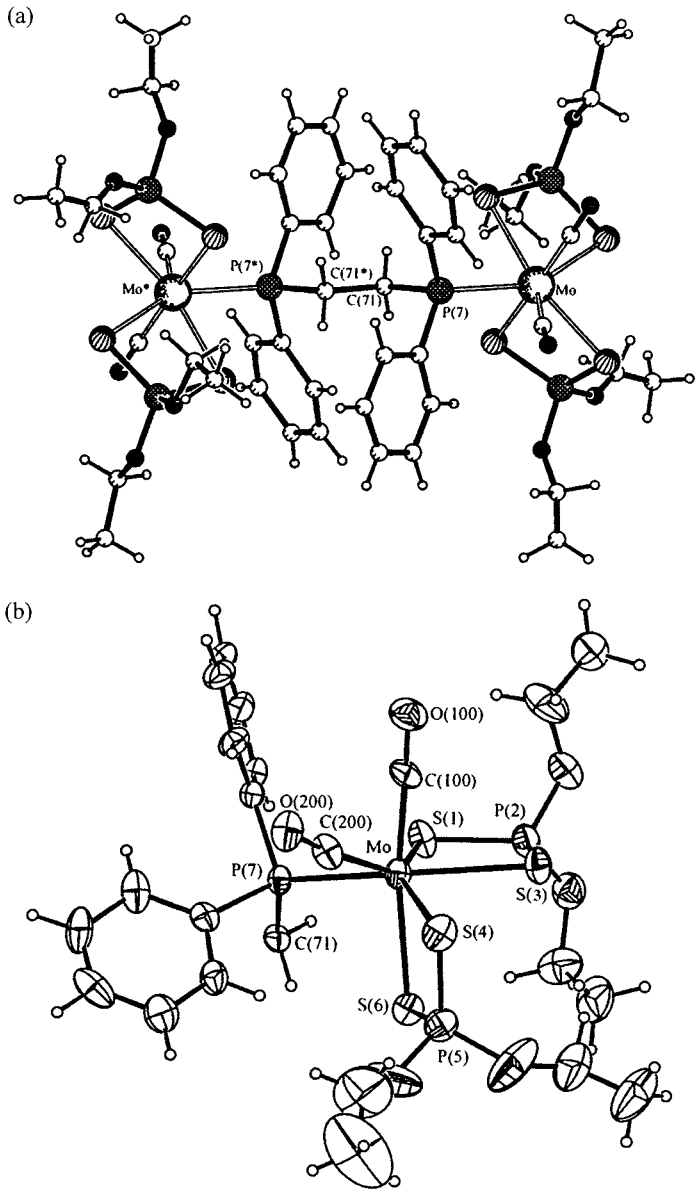

Fig. 2. The structure of $[Mo(CO)_2\{S_2P(OEt)_2\}]_2$(μ-dppe) (**3a**): (a) a PLATON view showing the centrosymmetric arrangement of two $Mo(CO)_2\{S_2P(OEt)_2\}$structural units linked by the dppe bridge; the symmetry operation * $-x+2$, $-y+1$, $-z+2$ is used to generate the equivalent atoms; (b) an ORTEP view of the asymmetric unit of **3a**, showing the molybdenum coordination. The thermal ellipsoids are drawn at 20% probability and the atom numbering scheme of the phenyl and ethoxy groups is omitted for clarity. The analogous tungsten complex **3b** is isomorphous.

[P(7)], −0.123(1) [P(9)], 0.357(1) [S(4)], −0.455(2) [S(1)] and 0.402(1) [S(3)] in **4a** and −0.448(2) [P(7)], 0.598(2) [P(10)], −0.466(2) [S(4)], 0.175(2) [S(1)] and 0.141(2) [S(3)] in **5a**. This distortion of the equatorial plane can be ascribed to the steric requirements of the bulky ligands, such as $S_2P(OEt)_2$ and dppm in **4a** or dppe in **5a**. On the other hand, the *cis* angles on the equatorial plane are close to the ideal value of 72°. The largest shift from this value is of 5.3° in **4a**, being reduced to only 2.6° in **5a**. It is noteworthy that in both cases this difference is due to the P–Mo–P chelating angle. The increased size of dppe in **5a** over dppm **4a** is reflected in the widening of the P–Mo–P angle: 66.70(8) in **4a** and 77.55(11)° in **5a**. This also affects most of the other angles subtended at the metal center, including those not involving the phosphorus atoms, which changed by ca. 3–16°. In both complexes, the Mo–S distance involving the axial sulfur is longer than the equatorial ones, by ca. 0.04 Å in **4a** and 0.06 Å in **5a**.

The crystal structure **7a** is built from an asymmetric unit composed of one discrete molecule of [Mo(O)(I)-(dppe)$\{S_2P(OEt)_2\}$]. The molecular structure of **7a** and the labelling scheme adopted are shown in Fig. 6. The bond lengths and angles listed in Table 4 indicate that

Table 2
Bond lengths (Å) and angles (°) in the metal coordination spheres of **6b**

Bond lengths			
W–C(100)	1.920(5)	W–C(200)	1.938(6)
W–S(1)	2.617(5)	W–S(4)	2.601(5)
W–S(6)	2.619(4)	W–P(7)	2.480(4)
W–P(10)	2.568(4)		
Bond angles			
S(4)–W–S(1)	78.9(2)	P(7)–W–S(4)	107.2(1)
P(7)–W–P(10)	75.5(1)	P(10)–W–S(1)	92.6(1)
P(7)–W–S(1)	159.2(1)	P(10)–W–S(4)	161.7(1)
C(100)–W–S(6)	159.0(6)	C(100)–W–C(200)	68.6(2)
C(200)–W–S(6)	131.9(2)	S(4)–W–S(6)	75.8(2)
C(100)–W–P(7)	115.8(2)	C(200)–W–P(7)	73.0(2)
C(100)–W–P(10)	83.5(2)	C(200)–W–P(10)	121.8(2)
C(100)–W–S(4)	110.3(2)	C(200)–W–S(4)	75.6(2)
P(7)–W–S(6)	79.6(1)	P(10)–W–S(6)	87.1(2)
C(100)–W–S(1)	78.8(2)	C(200)–W–S(1)	127.6(2)
S(6)–W–S(1)	82.9(1)		

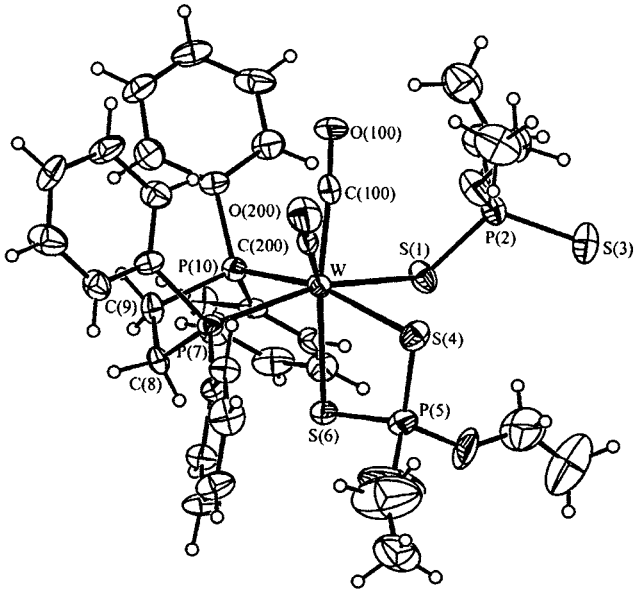

Fig. 3. An ORTEP view of $[W(CO)_2(dppe)\{S_2P(OEt)_2\}_2]$ (**6b**), with thermal ellipsoids drawn at 30% probability. The atom numbering scheme of the phenyl and ethoxy groups is omitted for clarity.

the molybdenum displays a distorted octahedral geometry with the equatorial plane defined by two sulfur atoms from the $S_2P(OEt)_2$ ligand and two phosphorus atoms from dppe. Six-coordination is completed axially by one iodine atom and one oxygen atom from an *oxo* group, with an I–Mo–O angle deviating from 180° by 12°. The *cis* angles are within 10° of the ideal octahedral value of 90°. The P–Mo–P angle is only slightly larger than that found for dppe in **6b** [75.5(1)°] and in **5a** [74.55(11)°]. The S–Mo–S angle of 79.12(10)° is also larger by ca. 4–3° than the equivalent angles reported for the previous structures. This comparison suggests that the value of these two chelating angles is imposed

Table 3
Bond lengths (Å) and angles (°) in the metal coordination sphere of **4a** and **5a**

	4a ($x = 9$)	**5a** ($x = 10$)
Bond lengths		
Mo–C(100)	1.904(8)	1.919(14)
Mo–S(1)	2.650(3)	2.670(4)
Mo–S(3)	2.618(3)	2.628(4)
Mo–S(4)	2.577(3)	2.579(4)
Mo–S(6)	2.688(3)	2.730(4)
Mo–P(7)	2.471(2)	2.526(4)
Mo–P(x)	2.462(2)	2.462(3)
Bond angles		
P(x)–Mo–P(7)	66.70(8)	74.55(11)
P(x)–Mo–S(4)	74.97(7)	73.98(13)
S(4)–Mo–S(1)	76.68(7)	73.70(13)
S(3)–Mo–S(1)	73.69(8)	73.39(10)
P(7)–Mo–S(3)	73.21(8)	73.18(9)
S(4)–Mo–S(6)	75.49(9)	74.75(10)
P(x)–Mo–S(6)	95.81(7)	109.80(2)
P(7)–Mo–S(4)	141.27(7)	136.96(10)
P(x)–Mo–S(3)	138.90(7)	139.44(11)
S(4)–Mo–S(3)	142.62(8)	145.86(11)
P(x)–Mo–S(1)	146.88(8)	138.87(10)
P(7)–Mo–S(1)	141.37(8)	145.66(11)
C(100)–Mo–P(7)	85.00(20)	99.30(30)
C(100)–Mo–P(x)	85.40(20)	77.90(30)
C(100)–Mo–S(4)	97.60(20)	101.90(30)
C(100)–Mo–S(3)	100.10(20)	83.80(30)
C(100)–Mo–S(1)	81.70(20)	84.60(30)
C(100)–Mo–S(6)	172.30(20)	169.90(30)
S(3)–Mo–S(6)	83.96(10)	93.72(11)
P(7)–Mo–S(6)	102.41(8)	89.27(9)
S(1)–Mo–S(6)	93.33(7)	85.27(10)

by the bite angles of the bidentate ligand, dppe or $S_2P(OEt)_2$. The bond distances Mo–S and Mo–P cannot be compared with those found for the related complexes described above, owing to the different formal oxidation states of the metal, namely IV in **7a** and II in all the remaining ones. These distances, as well as the distances Mo–I of 2.963(3) Å and Mo–O of 1.695(6) Å, are within the expected values [9].

In general, the M–S and M–P distances are comparable to those observed in related heptacoordinate Mo(II) and W(II) complexes, as described in Refs. [4d,4g,5a], for instance. It is more interesting to compare complexes **2a**, **2b**, **3a**, and **3b** with those described by Baker et al. [4h], which are hexacoordinate complexes containing two carbonyl groups, two monodentate phosphines and a bidentate dithiolate, and adopting a trigonal prismatic geometry. The Mo–S in particular are shorter (2.386–2.430 Å). These are formally 16 electrons species and it can be assumed that the sulfur ligand acts as a π-donor, leading to some double bond character and therefore a stronger M–S bond. In the saturated heptacoordinate complexes described in this work, this should not happen.

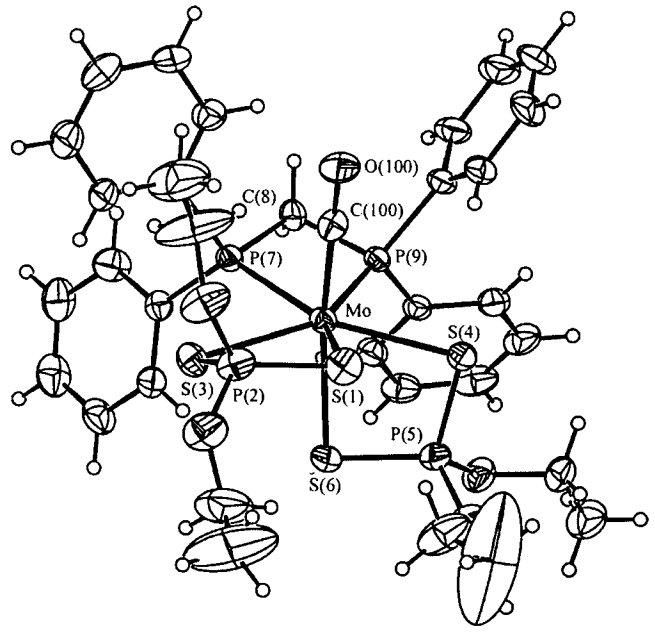

Fig. 4. An ORTEP view of $[Mo(CO)(dppm)\{S_2P(OEt)_2\}_2]$ (**4a**), with thermal ellipsoids drawn at 30% probability. The atom numbering scheme of the phenyl and ethoxy groups is omitted for clarity.

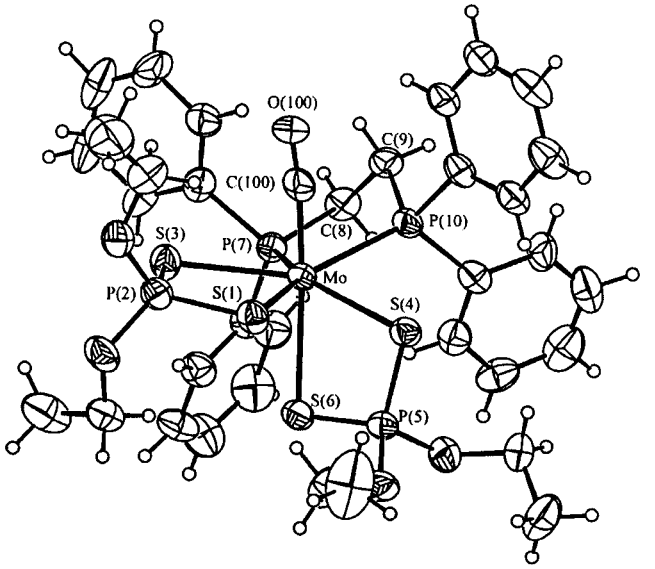

Fig. 5. An ORTEP view of $[Mo(CO)(dppe)\{S_2P(OEt)_2\}_2]$ (**5a**), with thermal ellipsoids drawn at 20% probability. The atom numbering scheme of the phenyl and ethoxy groups is omitted for clarity.

2.3. Cyclic voltammetry studies

The redox behavior of complexes $[Mo(CO)_2(PPh_3)\{S_2P(OEt)_2\}_2]$ (**2a**), $[W(CO)_2(PPh_3)\{S_2P(OEt)_2\}_2]$ (**2b**), $[Mo(CO)_2\{S_2P(OEt)_2\}_2]_2(\mu\text{-dppe})$ (**3a**), $[W(CO)_2\{S_2P(OEt)_2\}_2]_2(\mu\text{-dppe})$ (**3b**), $[Mo(CO)(dppm)\{S_2P(OEt)_2\}_2]$ (**4a**), $[Mo(CO)(dppe)\{S_2P(OEt)_2\}_2]$ (**5a**), and $[Mo(O)(I)(dppe)\{S_2P(OEt)_2\}]$ (**7a**), was studied in dichloromethane containing $[NBu_4][PF_6]$ as the supporting electrolyte. The cyclic voltammograms of **2a**, **2b**, **3a** and **3b** are similar, but the resolution is better in the case of the W complexes. The basic pattern consists of two irreversible oxidation processes, and an irreversible reduction wave.

Complex **4a** exhibits a slightly different behavior, which is not surprising owing to the different coordination environment of the metal. The two oxidations are observed at less positive potentials and the reduction counterparts are observed, although the processes are still by far irreversible. The same reductions at very negative potentials are found (-1408 mV). Complex **5a**, on the other hand, exhibits a quasi-reversible oxidation (210, 136 mV) superimposed in the usual pattern: two irreversible oxidations and an irreversible reduction.

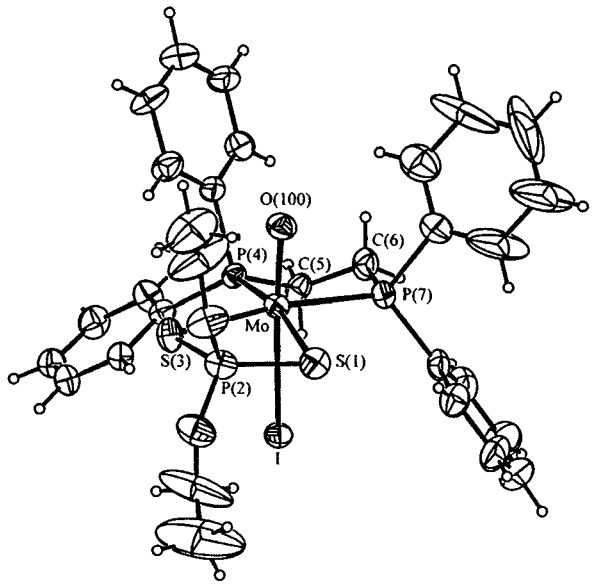

Fig. 6. An ORTEP view of $[Mo(O)(I)(dppe)\{S_2P(OEt)_2\}]$ (**7a**), with thermal ellipsoids drawn at 20% probability. The atom numbering scheme of the phenyl and ethoxy groups is omitted for clarity.

Table 4
Bond lengths (Å) and angles (°) in the metal coordination spheres of **7a**

Bond lengths			
Mo–O(100)	1.695(6)	Mo–I	2.963(3)
Mo–S(3)	2.496(3)	Mo–S(1)	2.507(3)
Mo–P(4)	2.509(2)	Mo–P(7)	2.529(3)
S(3)–Mo–S(1)	79.12(10)		
Bond angles			
O(100)–Mo–S(3)	99.5(3)	O(100)–Mo–S(1)	102.5(3)
O(100)–Mo–P(4)	91.1(3)	O(100)–Mo–P(7)	89.6(3)
S(3)–Mo–P(4)	97.9(1)	S(1)–Mo–P(4)	166.4(1)
S(3)–Mo–P(7)	170.7(1)	S(1)–Mo–P(7)	100.9(1)
P(4)–Mo–P(7)	70.0(1)	O(100)–Mo–I	167.8(2)
S(3)–Mo–I	89.4(1)	S(1)–Mo–I	87.2(1)
P(4)–Mo–I	79.4(1)	P(7)–Mo–I	81.3(1)

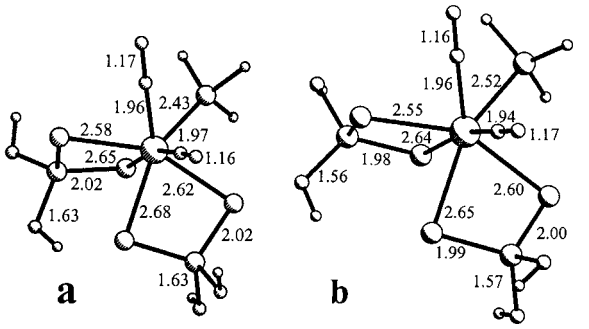

Fig. 7. The structure of model $[Mo(CO)_2(PH_3)\{S_2P(OH)_2\}_2]$ (**2a**): (a) optimized structure from DFT calculations; (b) X-ray structure with hydrogen atoms replacing ethyl and phenyl groups.

2.4. Theoretical calculations

DFT calculations [10] (ADF program [11]) were performed on several of the complexes (**2a**, **2b**, **3a**, **3b**, and **5a**; details in Section 4), in order to find some explanation for their redox behavior. **5a** differs from the other complexes as the geometry is a pentagonal bipyramid, rather than a capped octahedron. The phenyl groups of the amines, as well as the ethyl groups of the dithiophosphate, were replaced by hydrogen atoms, in order to reduce the size of the calculations. The structures of the models for complexes **2a** and **2b**, respectively $[Mo(CO)_2(PH_3)\{S_2P(OH)_2\}_2]$ and $[W(CO)_2(PH_3)\{S_2P(OH)_2\}_2]$, were fully optimized. The results are shown in Fig. 7 for the molybdenum complex and are analogous for tungsten. The calculated distances, angles, and the coordination environment (left) are very similar to the experimental X-ray structure with hydrogen atoms replacing alkyls and phenyls (right).

The differences are concentrated on the OH positions as quantified by the SPOH torsion angles, no doubt because of replacement of the bulky groups by –OH. However, these differences are so small with respect to the metal environment, that for the other complexes only single point calculations were carried out. The full optimization process was very slow owing to the requirement of optimizing the peripheric atoms, but these atoms did not contribute significantly to a better knowledge of the frontier orbitals. The energy and composition of the frontier orbitals of the complexes studied is given in Table 5.

The first conclusion is that the difference between Mo and W complexes, from comparing **2a** and **2b**, is much smaller than that produced by replacing a phosphine, keeping the octahedral capped coordination environment (**2a** and **3a**). The fourth complex, **5a**, exhibits a different geometry (pentagonal bipyramid), as well as containing only one carbonyl and a bidentate phosphine. It is not surprising that the energy and composition of the frontier orbitals for this complex are rather different from that of the others, the same happening with the redox behavior.

The two oxidations observed for the W complex **2b** can be assigned as metal oxidations, as both the HOMO and HOMO − 1 are strongly concentrated on the metal atom, as well as on the sulfur ligand and on the carbonyls. As these orbitals are bonding, the loss of an electron leads to bond weakening and further reaction, and the accompanying reduction is not observed. The reduction process starts by populating a level with less (but still significant) contribution of the metal, but more localized on all the ligands. Its metal–ligand antibonding character leads to further reactivity. The pattern is similar for the binuclear species **3a** and **3b**. In

Table 5
The energy (kJ mol^{-1}) and composition (%) of the frontier orbitals of model complexes **2a**, **2b**, **3a**, **3b**, and **5a**

Complex		Orbital	Energy	Composition (%)			
				Mo	$S_2P(OH)_2$	Phosphine	CO
$[Mo(CO)_2(PPh_3)\{S_2P(OH)_2\}_2]$	**2a**	HOMO − 1	−514.84	51.0	22.1	3.1	20.0
		HOMO	−501.65	45.5	26.2	4.4	20.1
		LUMO	−280.90	36.8	29.9	9.3	21.0
$[W(CO)_2(PPh_3)\{S_2P(OH)_2\}_2]$	**2b**	HOMO − 1	−504.44	49.3	20.1	3.8	23.2
		HOMO	−490.02	44.4	23.6	5.4	23.1
		LUMO	−263.97	29.5	28.0	11.5	28.0
$[Mo(CO)_2\{S_2P(OH)_2\}_2]_2(\mu\text{-dppe})$	**3a**	HOMO − 1	−482.46	48.4	18.1	1.4	22.9
		HOMO	−482.23	48.5	18.0	1.3	22.8
		LUMO	−283.13	34.7	26.4	10.4	20.1
$[W(CO)_2\{S_2P(OH)_2\}_2]_2(\mu\text{-dppe})$	**3b**	HOMO − 1	−469.28	47.1	17.2	1.9	25.6
		HOMO	−469.02	47.3	17.1	1.7	25.6
		LUMO	−266.41	30.2	23.5	12.8	23.8
$[Mo(CO)(dppe)\{S_2P(OH)_2\}_2]$	**5a**	HOMO − 1	−407.85	59.6	14.5	7.1	16.5
		HOMO	−386.03	58.3	14.9	10.9	13.0
		LUMO	−211.84	34.7	26.9	29.4	2.9

these, the HOMO and HOMO − 1 are very similar, owing to the dimeric nature of the complexes. The energies of the frontier orbitals are lower than for **2a**, suggesting more difficult oxidations and easier reductions. The almost degeneracy of the two highest levels makes direct comparison difficult. As far as reduction is concerned, however, the LUMO + 1 is similar to the LUMO, and the easiest reductions are indeed observed.

The different geometry of [Mo(CO)(dppe)-$\{S_2P(OEt)_2\}_2$] (**5a**), is reflected in the different energies and compositions of the frontier orbitals. The HOMO is much more localized on the metal and its energy is much higher than for the previous complexes. In this case, the first oxidation occurs at lower potentials and is reversible.

3. Conclusions

A family of complexes of Mo(II) and W(II) containing the dithiophosphate ligand and carbonyls or phosphines, displaying a coordination number seven, has been prepared and characterized. The coordination geometry adopted by the metal is either a capped octahedron, with a carbonyl ligand in the capping position, when two carbonyl groups are present, or a pentagonal bipyramid in the monocarbonyl derivative. The carbonyl group occupies one axial position. These complexes are relatively reactive, since irreversible processes are found to take place during cyclic voltammetric studies and a longer crystallization time led to the formation of an oxidized six-coordinate species.

4. Experimental

4.1. Synthesis

Commercially available reagents and all solvents were purchased from standard chemical suppliers. All solvents were used without further purification except MeCN (dried over CaH_2), CH_2Cl_2 (dried over CaH_2), and THF, which was distilled over sodium/benzophenone ketyl and used immediately. $NH_4[S_2P(OEt)_2]$ (Aldrich) was recrystallized from THF. The complexes $[MI_2(CO)_3(NCMe)_2]$ (M = Mo, W) were synthesized according to literature procedures [4a].

^{1}H-NMR spectra were recorded on a Bruker AMX-300 (300 MHz) spectrometer in d^3-CD_3CN (δ 1.93), using TMS as internal reference, and ^{31}P shifts were measured with respect to external 85% H_3PO_4. Elemental analyses were carried out at ITQB. The IR spectra were recorded on a Unicam Mattson 7000 FTIR spectrometer. Samples were run as KBr pellets.

4.2. Preparation of $[Mo(CO)_2(PPh_3)\{S_2P(OEt)_2\}_2]$ (2a)

$[MoI_2(CO)_3(NCMe)_2]$ (0.103 g, 0.2 mmol) was dissolved in CH_2Cl_2 (10 ml), and solid $NH_4[S_2P(OEt)_2]$ (0.084 g, 0.4 mmol) was added with vigorous stirring. The color of the solution changed from dark-red to red-brown, and a white precipitate formed gradually (30 min). The reaction mixture was filtered, solid PPh_3 (0.052 g, 0.2 mmol) was added to the red–brown filtrate, rapid gas evolution occurred, and the color of the solution immediately turned to red. The solution was stirred for further 30 min, and then concentrated to about one fourth of its original volume. Hexane (20 ml) was added, the solution was cooled down (−20 °C) overnight, to afford red crystals of the compound $[Mo(CO)_2(PPh_3)\{S_2P(OEt)_2\}_2]$ (**2a**). The yield was 0.13 g (83%). One of the crystals was used for a single crystal X-ray diffraction analysis.

Anal. Found: S, 16.05; C, 42.24; H, 4.19%. Calc. for $C_{28}H_{35}MoO_6P_3S_4$: S, 16.35; C, 42.87; H, 4.46%. ^{1}H-NMR: δ 7.41 (s, 15H, C_6H_5), 4.11 (s, 8H, OCH_2CH_3), 1.28 (s, 12H, OCH_2CH_3).

4.3. Preparation of $[W(CO)_2(PPh_3)\{S_2P(OEt)_2\}_2]$ (2b)

$[WI_2(CO)_3(NCMe)_2]$ (0.121 g, 0.2 mmol) was dissolved in CH_2Cl_2 (10 ml), and solid $NH_4[S_2P(OEt)_2]$ (0.084 g, 0.4 mmol) was added with vigorous stirring. The color of the solution changed from dark-red to orange, and a white precipitate formed gradually (30 min). The reaction mixture was filtered, solid PPh_3 (0.052 g, 0.2 mmol) was added to the filtrate, and the color of the solution turned to red quickly. The solution was stirred for further 30 min, and then concentrated to about one fourth of its original volume. Hexane (20 ml) was added, the solution was cooled down (−20 °C) overnight, to afford red crystals of the compound $[W(CO)_2(PPh_3)\{S_2P(OEt)_2\}_2]$ (**2b**). The yield was 0.14 g (80%). One of the crystals was used for a single crystal X-ray diffraction analysis.

Anal. Found: S, 14.46; C, 38.31; H, 3.67%. Calc. for $C_{28}H_{35}O_6P_3S_4W$: S, 14.70; C, 38.55; H, 4.01%. ^{1}H-NMR: δ 7.32–7.51 (m, 15H, C_6H_5), 4.14 (s, 8H, OCH_2CH_3), 1.26–1.37 (m, 12H, OCH_2CH_3).

The other Mo and W compounds, $[Mo(CO)_2\{S_2P(OEt)_2\}_2]$(μ-dppe) (**3a**) $[W(CO)_2\{S_2P(OEt)_2\}_2]$-(μ-dppe) (**3b**), $[Mo(CO)(dppm)\{S_2P(OEt)_2\}_2]$ (**4a**), $[W(CO)(dppm)\{S_2P(OEt)_2\}_2]$ (**4b**), [Mo(CO)(dppe)-$\{S_2P(OEt)_2\}_2$] (**5a**), $[W(CO)_2(dppe)\{S_2P(OEt)_2\}_2]$ (**6b**), $[Mo(O)(I)(dppe)\{S_2P(OEt)_2\}]$ (**7a**), were prepared in a similar way, and also crystallized in a similar way (except **7a**). All appeared as red crystals. The reactive mixture which gave **5a**, as we mentioned before, was put in a cold room (0 °C) for about 2 weeks, leading to **7a** as red–purple crystals.

4.4. $[Mo(CO)_2\{S_2P(OEt)_2\}_2](\mu\text{-dppe})$ (**3a**)

Anal. Found: S, 17.15; C, 37.98; H, 4.03%. Calc. for $C_{46}H_{64}Mo_2O_{12}P_6S_8$: S, 17.78; C, 38.25; H, 4.43%. ^{1}H-NMR: δ 7.55–7.62 (m, 20H, C_6H_5), 3.87–4.28 (m, 16H, OCH_2CH_3), 2.66–2.73 (m, 4H, CH_2CH_2 from dppe), 1.12–1.39 (m, 24H, OCH_2CH_3). Phosphine used: 0.040 g, 0.1 mmol. Weight of **3a**: 0.250 g. Yield 87%.

4.5. $[W(CO)_2\{S_2P(OEt)_2\}_2](\mu\text{-dppe})$ (**3b**)

Anal. Found: S, 16.06; C, 33.92; H, 3.73%. Calc. for $C_{46}H_{64}O_{12}P_6S_8W_2$: S, 15.81; C, 34.10; H, 3.95%. ^{1}H-NMR: δ 7.59 (s, 20H, C_6H_5), 3.96–4.24 (m, 16H, OCH_2CH_3), 2.66–2.72 (m, 4H, CH_2CH_2 from dppe), 1.22–1.37 (m, 24H, OCH_2CH_3). Phosphine used: 0.040 g, 0.1 mmol. Weight of **3b**: 0.230 g. Yield 71%.

4.6. $[Mo(CO)(dppm)\{S_2P(OEt)_2\}_2]$ (**4a**)

Anal. Found: S, 14.19; C, 43.54; H, 4.43%. Calc. for $C_{34}H_{42}MoO_5P_4S_4{\cdot}CH_2Cl_2$: S, 13.29; C, 43.62; H, 4.57%. ^{1}H-NMR: δ 7.42 (s, 20H, C_6H_5), 5.44 (s, 2H, CH_2Cl_2), 3.90–4.31 (m, 8H, OCH_2CH_3), 2.92 (s, 2H, CH_2 from dppm), 0.86–1.39 (m, 12H, OCH_2CH_3). Phosphine used: 0.077 g, 0.2 mmol. Weight of **4a**: 0.140 g. Yield 78%.

4.7. $[W(CO)(dppm)\{S_2P(OEt)_2\}_2]$ (**4b**)

Anal. Found: S, 12.90; C, 41.26; H, 4.27%. Calc. for $C_{34}H_{42}O_5P_4S_4W$: S, 13.25; C, 42.23; H, 4.35%. ^{1}H-NMR: δ 7.34–7.56 (m, 20H, C_6H_5), 4.02–4.79 (m, 8H, OCH_2CH_3), 3.28 (s, 2H, CH_2 from dppm), 0.86–1.36 (m, 12H, OCH_2CH_3). Phosphine used: 0.077 g, 0.2 mmol. Weight of **4b**: 0.140 g. Yield 71%.

4.8. $[Mo(CO)(dppe)\{S_2P(OEt)_2\}_2]$ (**5a**)

Anal. Found: S, 13.75; C, 48.10; H, 5.20%. Calc. for $MoC_{35}H_{44}O_5P_4S_4$: S, 14.34; C, 47.07; H, 4.93%. ^{1}H-NMR: δ 7.33–7.87 (m, 20H, C_6H_5), 3.85–4.42 (m, 8H, OCH_2CH_3), 2.67–2.73 (m, 4H, CH_2CH_2 from dppe), 1.16–1.48 (m, 12H, OCH_2CH_3). Phosphine used: 0.080 g, 0.2 mmol. Weight of **5a**: 0.250 g. Yield 87%.

4.9. $[W(CO)_2(dppe)\{S_2P(OEt)_2\}_2]$ (**6b**)

Anal. Found: S, 11.69; C, 40.51; H, 4.13%. Calc. for $C_{36}H_{44}O_6P_4S_4W{\cdot}CH_2Cl_2$: S, 11.71; C, 40.61; H, 4.21%. ^{1}H-NMR: δ 7.59 (s, 20H, C_6H_5), 5.44 (s, 2H, CH_2Cl_2), 3.87–4.04 (m, 8H, OCH_2CH_3), 2.66–2.71 (m, 4H, CH_2CH_2 from dppe), 1.16–1.28 (m, 12H, OCH_2CH_3). Phosphine used: 0.080 g, 0.2 mmol. Weight of **6b**: 0.230 g. Yield 71%.

4.10. $[Mo(O)(I)(dppe)\{S_2P(OEt)_2\}]$ (**7a**)

Anal. Found: S, 7.80; C, 44.96; H, 4.09%. Calc. for $C_{30}H_{34}IMoO_3P_3S_2$: S, 7.78; C, 43.78; H, 4.13%. ^{1}H-NMR: δ 7.37–7.86 (m, 20H, C_6H_5), 3.97–4.44 (m, 4H, OCH_2CH_3), 2.73–2.96 (m, 4H, CH_2CH_2 from dppe), 1.23–1.48 (m, 6H, OCH_2CH_3). ^{31}P{^{1}H}-NMR: δ 77.4 (s, $S_2P(OEt)_2$), 53.1 (s, dppe). Phosphine used: 0.080 g, 0.2 mmol. Weight of **6b**: 0.050 g. Yield 31%.

4.11. Crystal structure determinations

The pertinent crystal data and refinement details are listed in Table 6. The X-ray data for all complexes were collected on a MAR research plate system using graphite Mo–K_α radiation at Reading University. The crystals were positioned at 70 mm from the image plate. 95 frames were measured at 2° intervals using an adequate counting time between 2 and 5 min. Data analysis was carried out with the XDS program [12]. Intensities of the complexes **3a**, **3b**, **6b** and **7a** were corrected empirically for absorption effects with the DIFABS program [13].

The structures were solved by direct methods. All non-hydrogen atoms were refined with anisotropic thermal parameters. The hydrogen atoms were introduced in the refinement at the geometric idealized positions giving isotropic thermal parameters equal 1.2 times those of the carbon atom they were attached. Then, the structures were refined by full matrix least-squares on F^2 using a weighting scheme with a standard form until convergence. The X-ray determinations of **2b**, **4a**, **5a**, **6b**, and **7a** showed positive peaks for residual electronic density greater than 1 e Å^{-3}, but in all cases the corresponding peak was within the metal coordination sphere. The structure of **3b** shows a residual electronic density in the range -0.57–1.74 e Å^{-3}, with the positive peak of 1.46 Å having two coordinates equivalent to those of the tungsten atom.

All calculations required to solve and refine the structures were carried out with SHELXS and SHELXL from the SHELX97 package [14]. Molecular diagrams were performed with the PLATON graphical interface [15].

4.12. Electrochemistry

All electrochemical instrumentation was from BAS and consisted of a CV-50W Voltammetric Analyzer connected to a BAS/Windows data acquisition software and a three electrode VC-2 voltammetry cell assembly in a C-2 Cell Stand, enclosed in a Faraday Cage. Also from BAS were the MF-2013 Platinum Working electrode, MW-1032 Platinum Wire Auxiliary Electrode and MF-2079 Ag/AgCl Reference Electrode. The working electrode was polished on 1 mM diamond, then on alumina and finally sonicated. Between each CV scan it

Table 6
Crystal data and structure refinement details for complexes **2a**–**7a**

Compound	**2a**	**2b**	**3a**	**3b**	**4a**	**5a**	**6b**	**7a**
Empirical formula	$C_{28}H_{35}MoO_6P_3S_4$	$C_{28}H_{35}O_6P_3S_4W$	$C_{46}H_{64}Mo_2O_{12}P_6S_8$	$C_{46}H_{64}O_{12}P_6S_8W_2$	$C_{35}H_{44}Cl_2MoO_5P_4S_4$	$C_{35}H_{44}MoO_5P_4S_4$	$C_{37}H_{46}Cl_2O_6P_4S_4W$	$C_{30}H_{34}IMoO_3P_3S_2$
Formula weight	784.65	872.56	1443.15	1618.97	963.66	892.76	1093.61	822.44
Crystal system	monoclinic	monoclinic	monoclinic	monoclinic	monoclinic	triclinic	monoclinic	Monoclinic
Space group	$P2_1/n$	$P2_1/n$	$P2_1/c$	$P2_1/c$	$P2_1/n$	$P\bar{1}$	$P2_1/n$	$P2_1/n$
Unit cell dimensions								
a (Å)	9.850(13)	9.820(12)	15.330(20)	15.257(21)	10.580(11)	10.712(14)	21.226(27)	17.971(22)
b (Å)	23.871(27)	23.721(26)	11.255(17)	11.232(14)	20.740(16)	12.035(17)	11.128(15)	10.028(14)
c (Å)	15.482(17)	15.553(17)	19.827(29)	19.798(25)	20.152(20)	17.642(22)	21.703(25)	20.258(27)
α (°)						94.42(1)		
β (°)	95.52(1)	95.72(1)	110.10(1)	109.79(1)	99.59(1)	92.46(1)	117.11(1)	107.53(1)
γ (°)						113.57(1)		
V (Å^3)	3623	3605	3213	3192	4360	2072	4563	3481
Z	4	4	2	2	4	2	4	4
D_{calc} (Mg m^{-3})	1.438	1.608	1.492	1.684	1.468	1.431	1.590	1.569
$F(000)$	1608	1736	1476	1604	1976	920	2192	1640
Absorption coefficient (mm^{-1})	0.761	3.606	0.851	4.064	0.800	0.711	3.013	1.550
θ range (°)	2.16–26.07	2.16–26.08	2.11–26.08	2.12–25.90	1.96–26.12	1.86–25.96	2.14–26.19	2.11–25.96
Index ranges hkl	$0 \le h \le 11$	$0 \le h \le 11$	$0 \le h \le 18$	$-18 \le h \le 17$	$0 \le h \le 12$	$0 \le h \le 13$	$0 \le h \le 26$	$-22 \le h \le 22$
	$-29 \le k \le 29$	$-28 \le k \le 28$	$-13 \le k \le 13$	$0 \le k \le 13$	$-25 \le k \le 25$	$-13 \le k \le 13$	$0 \le k \le 12$	$0 \le k \le 11$
	$-19 \le l \le 18$	$-19 \le l \le 18$	$-24 \le l \le 22$	$-24 \le l \le 24$	$-24 \le l \le 2$	$-21 \le l \le 21$	$-26 \le l \le 23$	$-24 \le l \le 24$
Reflections collected	9602	11536	8821	9516	15163	6571	8099	
Unique reflections (R_{int})	5759 (0.0469)	6344 (0.0306)	5563 (0.0956)	5648 (0.0482)	7925 (0.0303)	6571 (0.0000)	8099 (0.0000)	10 002 (0.0504)
Data/restraints/parameters	5759/0/383	6344/0/366	5563/0/336	5648/0/332	7925/0/465	6571/0/440	8099/0/473	6100/0/352
Goodness-of-fit on F^2	1.121	1.111	0.967	1.020	1.064	0.952	1.538	1.078
Final R indices [$I > 2\sigma(I)$] R_1 and wR_2	0.0671, 0.1551	0.0535, 0.1176	0.0820, 0.1977	0.0562, 0.1202	0.0795, 0.1817	0.1024, 0.2404	0.0975, 0.3207	0.0730, 0.2136
R indices (all data) R_1 and wR_2	0.1181, 0.1762	0.0722, 0.1308	0.2550, 0.2507	0.1157, 0.1388	0.1090, 0.1967	0.1999, 0.2845	0.1197, 0.366	0.1218, 0.2501
Largest difference peak and hole (e Å^{-3})	0.551/−0.823	1.858/−2.031	0.550/−0.668	1.741/−0.574	1.888/−0.709	1.604/−1.395	2.934/−3.003	1.784/−1.340

was electrocleaned as a routine procedure. All experiments were run under Argon and at room temperature (23 ± 2 °C). Solutions were typically 1 mM in solute and 0.1 M in supporting electrolyte, tetrabutylammonium hexafluorophosphate (Aldrich), which was recrystallized from EtOH. Potentials were referred to the Ag | AgCl electrode, which was calibrated with a ferrocene solution [16].

4.13. DFT calculations

Density functional calculations [10] were carried out with the Amsterdam Density Functional (ADF1999) program developed by Baerends and coworkers [11]. Vosko, Wilk and Nusair's local exchange correlation potential was used [17]. Gradient corrected geometry optimizations [18] were performed using the Generalized Gradient Approximation (Becke's exchange [19] and Perdew's [20] correlation functionals), and included relativistic effects, treated by the ZORA formalism [21].

The inner shells of W ([1-5]s, [2-5]p, [3-4]d), Mo ([1-4]s, [2-4]p, 3d), C (1s), O (1s), P (1s, 2s, 2p) and S (1s, 2s, 2p) were frozen. An uncontracted triple-ζ nd, $(n+1)$s STO basis set was used for W and Mo augmented by one $(n+1)$p function. The valence shells for C, N, O (2s, 2p), and P, S (3s, 3p) were described by an uncontracted triple-ζ STO basis set, augmented by two polarization functions: 3d and 4f. For H, an uncontracted triple-ζ STO basis set (1s) with two polarization functions 2p and 3d was used. The full geometry optimizations were performed without any symmetry constraints.

The structure of the complex $[Mo(CO)_2(PPh_3)\{S_2P(OEt)_2\}_2]$ (**2a**), described above was used to build a model for the full optimization of the geometry, by replacing both ethyl and phenyl groups by hydrogen atoms, for both the Mo and the W derivative (**2a** and **2b**). For complexes **3a**, **3b**, and **5a**, single point calculations were performed, since the full optimization is very slow and the results obtained with **2a** showed a very good agreement between the calculated and the experimental structures in what concerns the metal coordination sphere.

5. Supplementary material

Crystallographic data for the structural analyses have been deposited with the Cambridge Crystallographic Data Centre, CCDC nos. 159787 (**2a**), 159788 (**2b**), 159789 (**3a**), 159790 (**3b**), 159791 (**4a**), 159792 (**5a**), 159793 (**6b**) and 159794 (**7a**). Copies of this information may be obtained free of charge from The Director, CCDC, 12 Union Road, Cambridge CB2 1EZ, UK (Fax: +44-1223-336033; e-mail: or www: http://www.ccdc.cam.ac.uk).

Acknowledgements

We thank Zara Miravent Tavares for the elemental analysis (ITQB) and cyclic voltammetric experiments. H.L. thanks Praxis XXI for a postdoctoral grant. V.F. thanks FCT for a sabbatical leave grant. The University of Reading and EPSRC are thanked for funds for the Image Plate system.

References

[1] (a) J. Kim, D.C. Rees, Science 257 (1992) 1677;
(b) W.-H. Orme-Johnson, Science 257 (1992) 1639;
(c) J. Kim, D.C. Rees, Nature 360 (1992) 553.
[2] J.J.R. Fraústo da Silva, R.J.P. Williams, The Biological Chemistry of the Elements, Clarendon Press, Oxford, 1991.
[3] H. Topsøe, B.S. Clausen, F.E. Massoth, Hydrotreating catalysis, in: J.R. Anderson, M. Boudart (Eds.), Catalysis–Science and Technology, vol. 11, Springer-Verlag, Berlin, 1996.
[4] (a) P.K. Baker, A. Bury, J. Organomet. Chem. 359 (1989) 189;
(b) P.K. Baker, M. van Kampen, D. ap Kendrick, J. Organomet. Chem. 421 (1991) 241;
(c) P.K. Baker, M.B. Hursthouse, A.I. Karaulov, A.J. Lavery, K.M. Abdul Malik, D.J. Muldoon, A. Shawcross, J. Chem. Soc. Dalton Trans. (1994) 3493;
(d) P.K. Baker, A.I. Clark, M.G.B. Drew, M.C. Currant, R.L. Richards, Polyhedron 17 (1998) 1407;
(e) N.G. Aimeloglu, P.K. Baker, M.M. Meehan, M.G.B. Drew, Polyhedron 17 (1998) 3455;
(f) P.K. Baker, L.A. Latif, M.M. Meehan, S. Zanin, M.G.B. Drew, Polyhedron 18 (1999) 257;
(g) P.K. Baker, M.G.B. Drew, A.W. Johans, U. Haas, L.A. Latif, M.M. Meehan, S. Zanin, J. Organomet. Chem. 590 (1999) 77–87;
(h) P.K. Baker, A.I. Clark, M.G.B. Drew, M.C. Durrant, R.L. Richards, Inorg. Chem. 38 (1999) 821.
[5] (a) G. Barrado, D. Miguel, J.A. Pérez-Martinez, V. Riera, J. Organomet. Chem. 463 (1993) 127–133;
(b) G. Barrado, D. Miguel, S. García-Granda, V. Riera, J. Organomet. Chem. 489 (1995) 129;
(c) G. Barrado, M.M. Hricko, D. Miguel, V. Riera, H. Wally, S. García-Granda, Organometallics 17 (1998) 820.
[6] (a) B. Zhuang, L. Huang, L. He, Y. Yuang, J. Lu, Inorg. Chim. Acta 145 (1988) 225–229;
(b) K.-B. Shiu, S.-M. Peng, M.-C. Cheng, S.-L. Wang, F.-L. Liao, J. Organomet. Chem. 461 (1993) 111;
(c) M. Cano, M. Panizo, J.A. Campo, J. Tornero, N. Menéndez, J. Organomet. Chem. 463 (1993) 121;
(d) K.-H. Yih, G.-H. Lee, Y. Wang, J. Organomet. Chem. 588 (1999) 125.
[7] (a) M.G.B. Drew, Seven-coordination chemistry, in: S.J. Lippard (Ed.), Progress in Inorganic Chemistry, vol. 23, Wiley, New York, 1977;
(b) R. Hoffmann, B.F. Beier, E.L. Muetterties, A.R. Rossi, Inorg. Chem. 16 (1977) 511.
[8] H. Liu, V. Félix, M.G.B. Drew, M.J. Calhorda, submitted.
[9] F.H. Allen, J.E. Davies, J.J. Galloy, O. Johnson, O. Kennard, C.F. Macrae, E.M. Mitchell, G.F. Mitchel, J.M. Smith, D.G. Watson, J. Chem. Inf. Comp. Sci. 31 (1991) 187.
[10] R.G. Parr, W. Yang, Density Functional Theory of Atoms and Molecules, Oxford University Press, New York, 1989.
[11] (a) E.J. Baerends, A. Bérces, C. Bo, P.M. Boerrigter, L. Cavallo, L. Deng, R.M. Dickson, D.E. Ellis, L. Fan, T.H. Fischer, C.

Fonseca Guerra, S.J.A. van Gisbergen, J.A. Groeneveld, O.V. Gritsenko, F.E. Harris, P. van den Hoek, H. Jacobsen, G. van Kessel, F. Kootstra, E. van Lenthe, V.P. Osinga, P.H.T. Philipsen, D. Post, C.C. Pye, W. Ravenek, P. Ros, P.R.T. Schipper, G. Schreckenbach, J.G. Snijders, M. Sola, D. Swerhone, G. te Velde, P. Vernooijs, L. Versluis, O. Visser, E. van Wezenbeek, G. Wiesenekker, S.K. Wolff, T.K. Woo, T. Ziegler, ADF, 1999;
(b) C. Fonseca Guerra, O. Visser, J.G. Snijders, G. te Velde, E.J. Baerends, Parallelisation of the Amsterdam Density Functional Programme, in: E. Clementi, C. Corongiu (Eds.), Methods and Techniques for Computational Chemistry, STEF, Cagliari, 1995, pp. 303–395;
(c) C. Fonseca Guerra, J.G. Snijders, G. te Velde, E.J. Baerends, Theor. Chem. Acc. 99 (1998) 391;
(d) E.J. Baerends, D. Ellis, P. Ros, Chem. Phys. 2 (1973) 41;
(e) E.J. Baerends, P. Ros, Int. J. Quantum Chem. S12 (1978) 169;
(f) P.M. Boerrigter, G. te Velde, E.J. Baerends, Int. J. Quantum Chem. 33 (1988) 87;
(g) G. te Velde, E.J. Baerends, J. Comp. Phys. 99 (1992) 84.
[12] W. Kabsch, J. Appl. Crystallogr. 21 (1988) 916.
[13] N. Walker, D. Stuart, DIFABS, Acta Cryst. Sect. A 39 (1983) 158.
[14] (a) G.M. Sheldrick, SHELX-86, Acta Crystallogr. Sect. A 46 (1990) 467;
(b) G.M. Sheldrick, SHELX-97, University of Göttingen, Göttingen, Germany, 1997.
[15] A.L. Spek, PLATON, A Multipurpose Crystallographic Tool, Utrecht University, Utrecht, The Netherlands, 1999.
[16] I.V. Nelson, R.T. Iwamoto, Anal. Chem. 35 (1963) 867.
[17] S.H. Vosko, L. Wilk, M. Nusair, Can. J. Phys. 58 (1980) 1200.
[18] (a) L. Versluis, T. Ziegler, J. Chem. Phys. 88 (1988) 322;
(b) L. Fan, T. Ziegler, J. Chem. Phys. 95 (1991) 7401.
[19] A.D. Becke, J. Chem. Phys. 88 (1987) 1053.
[20] (a) J.P. Perdew, Phys. Rev. B33 (1986) 8822;
(b) J.P. Perdew, Phys. Rev. B34 (1986) 7406.
[21] E. van Lenthe, A. Ehlers, E.-J. Baerends, J. Chem. Phys. 110 (1999) 8943.